In-situ study of catalytic CO oxidation on ultrathin MgO film supported Pd nanoparticles by Sum frequency generation: size and site effect

Jijin Wang, Aimeric Ouvrard, Wanquan Zheng, Serge Carrez, Ahmed Ghalgaoui, Bernard Bourguignon

In-situ study of catalytic CO oxidation on ultrathin MgO film supported Pd nanoparticles by Sum frequency generation: size and site effect

Jijin Wang, Aimeric Ouvrard, Wanquan Zheng, Serge Carrez, Ahmed Ghalgaoui and Bernard Bourguignon*

Institut des Sciences Moléculaires d'Orsay, CNRS, Université Paris-Saclay, 91405, Orsay, France

Abstract: Controlling reactive sites of nanoparticles (NPs) is crucial to improve catalyst efficiency. In this work, Sum-Frequency Generation is used to probe CO vibrational spectra on MgO(100) ultrathin film/Ag(100) supported Pd nanoparticles (NP) ranging from 3 to 6 nm in diameter and compared to coalesced Pd NPs and Pd(100) single crystal. We aim at *in-situ* evidencing the role played by active adsorption sites on the catalytic CO oxidation reactivity trends varying with NP size. From ultrahigh vacuum to the mbar range and temperatures from 293 K to 340 K, our observations suggest that bridge sites are the main active sites for CO adsorption and catalytic oxidation. On Pd(100) single crystal at 293 K, CO oxidation predominates over CO poisoning for pressure ratio of O_2/CO larger than 300; on Pd NPs, both the site coordination due to NP geometry and MgO support-induced (MgO-induced) Pd-Pd interatomic distance change, impact the reactivity trend varying with size in different ways. Edge sites with a low coordination are more reactive than facet sites, while facet with a smaller Pd-Pd atomic length is more reactive than that with a larger one. The interplay of both site and size effects gives rise to a non-monotonic reactivity trend of CO on MgO(100) ultrathin film supported Pd NPs: the reactivity of Pd NPs increases for smaller NP size side due to a higher edge/facet ratio and meanwhile increases for larger NP size

side due to the terrace facet with a smaller Pd-Pd atomic length at the NP surface and a lower diffusion barrier.

Key words: carbon monoxide, catalytic oxidation, Pd nanoparticle size, adsorption site, sum frequency generation, in-situ measurement

Corresponding Author: wangjij@lzu.edu.cn

Present Address: School of Nuclear Science and Technology, Lanzhou University, China

1. Introduction

Heterogeneous catalysts are materials with complex multicomponent, whose chemical and structural composition can be effectively changed to enable high selectivity and reaction rates [**1**]. However this large structural and chemical complexity of catalysts, such as particle morphology, size, oxide support etc…, impedes a detailed understanding of structure-reactivity relationships in the catalysis processes, which limits rational design of new catalytic materials [**2**]. The catalytic oxidation of carbon monoxide (CO) on transition metallic nanoparticles (NPs) has attracted attentions in the past decades for industrial applications for instance, in conversion of automobile exhaust or in fuel cells [**3**], but has also become a model probe to investigate the effect of geometry, adsorption sites, oxide support, on the reaction rates of metal NP catalysts [**2-12**]. Among metal NP catalysts for CO oxidation, Pt-group metals, especially Pt, including Pd [**13-18**], are the most commonly used thanks to their high catalytic activity.

The catalytic activity of Pd strongly depends on the oxidation state of Pd [**3,20**]. On Pd single crystal, O_2 can adsorb and dissociate (O(ad)) even at temperature as low as 200 K [**21**]. In addition to O(ad), Pd and O can interact in various ways at surface or subsurface to form PdO surface or

bulk oxides, which strongly influence CO combustion efficiency [**22-25**]. Systematic studies [**18**] have identified that O(ad) is the most reactive species on both Pd(111) and Pd(100) surfaces [**18,19,22**], followed by the reactivity of surface oxide Pd_5O_4 on Pd(111), which reacted with CO at a higher temperature (330 K compared to 223 K for CO oxidation on O(ad)/Pd(111), and bulk oxide PdO (react with CO from 493 K) [**18,22**].

The size effect of metal catalyst, from single atom to clusters, nanoparticles and even single crystal, plays a key role in catalytic reactivity [**12,26**]. The size effect for NPs deserved many studies because of its complexity: the size dependent adsorption sites (edge, facet, defects), the different coordination and electronic structures [**7**], and the atomic distance within the NP, strongly impact on the activation energy of adsorbed reactants [**2,10,12,29**]. Compared to Au NPs, which becomes more reactive for very small size (<2-3nm) [**6,7**], size effect for small Pd NPs (few nm) is still ambiguous [**22**]. Sitja *et al.* have shown that single atom of Pd are less reactive than few atom catalysts [**27**], Freund *et al.* have reported an activation energy for CO oxidation of 57-62 $kJ \cdot mol^{-1}$ on alumina supported 5 nm large Pd NPs [**28**], perfectly agreeing with the activation barrier energy found on Pd(111) of 59 ± 8 $kJ \cdot mol^{-1}$ [**30**]. In this case, the barrier energy was not affected by size reduction from single crystal to nanoparticle. However, Stará *et al.* have reported a strong decrease of the activation energy with decreasing particle size: 45-64 $kJ \cdot mol^{-1}$ for Pd(111), 32-45 $kJ \cdot mol^{-1}$ for 27 nm, and 19-20 $kJ \cdot mol^{-1}$ for 2.5 nm Pd NPs on Al_2O_3 [**31**]. Henry and co-workers have observed an increase of CO binding energy of more than 33.5 $kJ \cdot mol^{-1}$ for 2 nm NPs on MgO(100) compared to Pd single crystal [**32**]. In contrast, Stará *et al.* have reported a decrease of CO binding energy by 11 $kJ \cdot mol^{-1}$ for 2.5 nm NPs on Al_2O_3 compared to Pd(111) single crystal [**33**]. Direct calorimetric measurements of CO heat of adsorption have demonstrated a reduction by 42 $kJ \cdot mol^{-1}$ for 1.8 nm NPs on Fe_3O_4/Pt(111) film compared to Pd(111) [**34**]. Therefore a more

unambiguous picture of the role of size and adsorption site effects of Pd NPs is still missing for this system. To well monitor the role of different components in catalysis processes, the *in-situ/operando* characterization of catalytic reaction is needed [**12**].

Sum frequency generation (SFG) has proved over the past three decades to be a powerful and versatile spectroscopic probe for surfaces and interfaces, because of its high sensitivity, selectivity and capacity to determine molecular orientation, conformational structure adsorption sites and to follow vibrational dynamics and surface diffusion [**5, 35-39**]. SFG is particularly well suited for *in-situ* and *operando* heterogeneous catalysis study, which could be at high temperature, high pressure, in solution or on various surface morphology. With SFG vibrational spectroscopy, Rupprechter *et al.* have characterized the reaction of small molecules (CO, ethylene, ethene, methanol etc.) on various metal (Pd, Pt, Rh, Au, Ru, etc.) single crystal and oxide supported NPs at pressures ranging from UHV to 1 bar [**40, 41**]. Somorjai *et al.* have worked on catalytic reaction of organic molecules on oxide supported NPs at solid–gas and solid–liquid interfaces [**42, 43**]. In this work, using SFG spectroscopy we detect *in-situ* CO stretching vibrational mode on the Pd(100) single crystal and size-dependent Pd NPs on MgO/Ag(100) in order to investigate the role of adsorption sites (edge/facet, bridge/linear) and of Pd-Pd distance in catalytic activity trends varying with NP size .

2. Experimental setup

Sample growth and spectroscopy experiments were performed in an ultra-high vacuum chamber with a base pressure of 2×10^{-10} mbar. A mechanically polished Pd(100) single crystal was cleaned by repeated cycles of 30 min Ar^+ sputtering (600 eV, $1-2\times10^{-6}$ mbar, 5−7 μA) with the sample temperature kept at 600 K, followed by a first annealing at 1070 K for 5 min and a

second one at 670 K under ~5 Langmuir (1 L = 10^{-6} torr·sec) of O_2 (2×10^{-8} mbar, 5 min). A mechanically polished Ag(100) single crystal was cleaned by cycles of Ar^+ sputtering (600 eV, $1-2\times10^{-6}$ mbar, 20-30 μA) for 30 min followed by 10 min annealing at 800 K. The quality of the single-crystal and cleanliness was confirmed by LEED and APS. Two effusion cells were used for evaporation of Mg (550 K, 0.25 monolayer (ML) per min) and Pd (1420 K, 0.2 ML/min). A 3 ML thick MgO thin film has been epitaxially grown on Ag(100). Details of MgO film growth and quality optimization are given elsewhere [**44**]. Pd NPs were grown onto the MgO film by evaporating Pd with equivalent thickness ranging from 1 to 16 ML at 480 K. The Pd NPs characterization information can be found in Figure 1 of Ref. [**10**]. CO and O_2 pressures were ranging from 10^{-9} to 1 mbar.

Vibrational SFG system is used to probe internal CO stretch vibration signals. A super-continuum seeded BBO optical parametric amplifier (Spectra Physics, USA) pumped by a 800 nm Ti:Sa laser/amplifier system (Coherent, USA), with duration 120 fs, repetition rate 1 kHz, and energy 800 μJ/pulse, is used for SFG experiments. SFG emission is induced by two p−polarized collinear laser beams (high hyperpolarizability on metal surfaces), i.e., a near-infrared pulse, called "visible"(ω_{VIS} = 12376 cm^{-1}, 7 cm^{-1} fwhm, 3 ps duration, 2 μJ), and an infrared pulse (ω_{IR}=1950 cm^{-1}, ~150 cm^{-1} fwhm, 140 fs duration, 3 μJ) covering the spectral region of CO internal stretch frequencies (1800-2100 cm^{-1}), that are spatially (150 μm spot) and temporally overlapped on the surface sample [**10**,**45**]. Spatial overlap is obtained in collinear propagation after recombination of the visible and IR beams with a ZnSe plate treated to maximize the visible reflection. The visible pulse spectrum (width and position) is made by a home-made 4f pulse shaper including a single combination of lens (f=10 cm) and grating, a plane mirror and in front of it a slit which selects a small portion (2.5–10 cm^{-1}) of the visible pulse spectrum [**64**]. The incident angle of visible and

IR beams relative to the sample normal is 60^{o}. SFG spectra of CO were recorded during the experiment with a 1 min acquisition time per spectrum. During all the SFG experiment, the laser beams intensities were not changed, therefore the laser-induced molecular desorption can be ruled out [**45**]. All spectra were normalized to a SFG spectrum on a GaAs reference sample recorded in parallel data acquisition mode. In the conducted SFG experiments on Pd(100) single crystal, to avoid CO surface poisoning, the cleaned sample was pre-treated by O_2 at 10^{-5} mbar at 300 K during 20 min prior exposing to CO. O_2 pressure remained fixed at 10^{-5} mbar during experiments and CO pressure was varied to observe the corresponding CO spectra. For MgO/Ag(100) supported Pd NPs, the sample was pre-treated with 1.0×10^{-4} mbar O_2 for 20 min at 300 K, and then the O_2 pressure was decreased to 2.0×10^{-5} mbar prior to introducing CO at 1.0×10^{-4} mbar. Afterwards, the O_2 pressure was increased until the CO band disappears finally. If CO band persists at 1 mbar pressure of O_2, the sample was heated to oxidize the remaining CO. The temperature of sample is measured by an optical pyrometer IIRcon Modline 5.

3. Results and Discussion

CO oxidation on Pd(100) single crystal

With our present system, Pd NPs epitaxially grown on MgO/Ag(100) exhibit a (100) top facet [**46, 47**], motivating us to conduct a comparative study of the CO oxidation on Pd(100) single crystal.

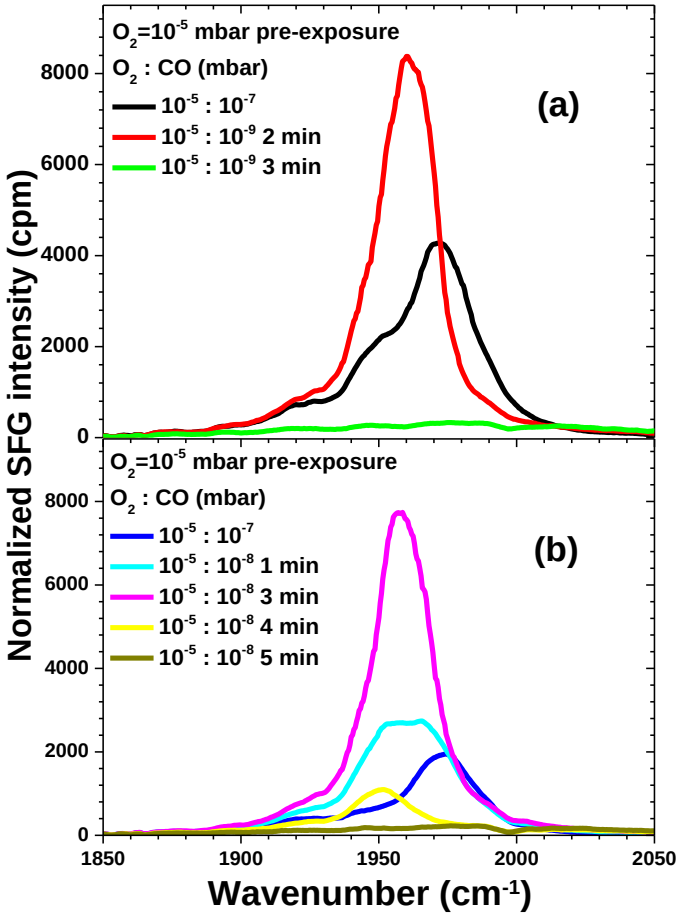

Figure 1. SFG spectra of CO internal stretch for various mixture ratios of static pressure of CO and O_2. Pd(100) single crystal surface is pre-exposed to O_2 at 10^{-5} mbar and to 10^{-7} mbar of CO at 293 K (t=0 min). Then CO pressure is decreased from 10^{-7} to (a) 10^{-9} mbar or (b) 10^{-8} mbar, respectively, spectra are recorded until CO bands vanish.

Figure 1a and **b** show the dynamics of CO vibrational band on Pd(100) when the CO pressure is decreased from 10^{-7} mbar to 10^{-9} mbar or 10^{-8} mbar respectively, while the pressure of O_2 is fixed at 10^{-5} mbar. Under 10^{-7} mbar of CO and 10^{-5} mbar of O_2, a single bridge adsorption CO vibrational band is observed at 1972 cm^{-1} (black and blue in **Figure 1a** and **b**, respectively) in agreement with previous results for CO/Pd(100) [**45**]. It corresponds to a coverage of CO close to ~0.67 ML, indicating that this O_2/CO ratio is too low to reduce CO coverage by oxidation and to avoid CO poisoning of the surface. Then, as shown in **Figure 1a** the red curve, CO pressure is

decreased to 10^{-9} mbar, which decreases CO coverage from 0.67 to around 0.5 ML (the CO band peak intensity will reach the maximum value at 0.5 ML coverage [**45**]) within 2 min. The CO band intensity at 0.5 ML coverage is higher than which at 0.67 ML because in the former case only the 'uncompressed' CO exist, however when the CO coverage extends more than 0.5 ML, another type of 'compressed' CO, with a hyperpolarizability which is half of the 'uncompressed' CO, appear and increase quickly. SFG intensity therefore decreases quickly when compressed CO coverage increases [**45**]. 1 min later the CO band has disappeared (green in **Figure 1a**), while in the presence of CO without O_2 at this pressure, the coverage is larger than 0.5 ML [**45**]. This disappearance of CO is attributed to CO oxidation because O(ad) can oxidize CO on Pd single crystal at temperature as low as 200K [**18,19,22**], while surface Pd oxide is excluded on Pd(100) as it requires a surface temperature higher than 190 °C at a higher O_2 pressure (0.26 mbar) [**48**]. Due to the fast reaction kinetics at this pressure compare to SFG measurement time only one intermediate point is recorded. In **Figure 1b**, CO pressure is decreased from 10^{-7} mbar to 10^{-8} mbar. Within 3 min CO coverage has decreased from 0.67 (blue) to ~0.5 ML (pink) and more than 2 min later the band has completely disappeared (dark yellow). From these two experiments, we can estimate the CO oxidation rate around 0.5 ML/min while CO adsorption rate at 10^{-8} mbar is approximately 0.17 ML/min. The full details of the calculation are given in **Supporting Information**.

From **Figure 1** it is found that CO poisoning hinders oxygen adsorption only when CO coverage is larger than 0.5 ML. Below this coverage, O_2 adsorption and dissociation occur and CO oxidation is observed at room temperature on Pd(100), as shown by the rapid decrease of SFG signal. Although the CO adsorption phase being compressed above 0.5 ML, the quick decrease of CO coverage under 10^{-8} mbar indicates that the Pd(100) surface is still reactive, implying that O(ad)

atoms can be formed without perturbing the CO compressed phase. Indeed well-ordered structures of co-adsorbed CO+O have been reported on different metals where the CO coverage is as large as that in the absence of oxygen [**51,52**]. CO oxidation process can prevail CO re-adsorption, provided that the pressure ratio O_2/CO is larger than 10^3. With a smaller ratio, CO adsorption process is faster than oxidation, so Pd(100) surface becomes rapidly poisoned by CO. This limitation to the pressure ratio above 10^3 holds at room temperature and O_2 pressure up to 10^{-3} mbar according to our experiments. It is known that at higher temperature (>500 K), the onset of CO desorption will keep the CO coverage below saturation of the adsorption phase (<0.5 ML), allowing O adsorption, which enables to use pressure ratio O_2/CO close to unity [**41**].

CO oxidation on MgO ultrathin-film-supported Pd nanoparticles

SFG spectra of CO at 10^{-4} mbar for increasing oxygen pressures on Pd NPs on MgO/Ag(100) with different equivalent thicknesses (16 ML, 4 ML and 1 ML corresponding to coalesced, 5.8 nm and 3.6 nm average diameter NPs, respectively [**10**]) are shown in **Figure 2**. CO oxidation process on Pd(100) are shown in **Figure S2** and can be directly compared to 16 ML Pd NPs. The main internal stretch CO vibrational band ranging from 1930 to 1980 cm^{-1} depending on NPs size is attributed to the bridge-site adsorption of CO on (100) facets or edges of the NP [**10**]. A contribution of CO bridge bonded on (111) cannot be excluded, as they fall in the same spectral region, but considering NP geometry and SFG selection rules, they are expected to have a weaker contribution in SFG spectra. In addition, two very weak bands at 2055 and 2090 cm^{-1}, not observed on Pd(100) single crystal, are present for 4 ML and 1 ML Pd NPs and attributed to linear CO located at edges or defects [**9**] and linear CO band on (111) facets [**10, 53**], respectively. Linear CO absorption on (111) facets is still weak at 10^{-4} mbar pressure.

The frequency of CO band in the case of O+CO co-adsorption (black in **Figure 2a,b and c**) is redshifted compared with which without O (dots). As shown in **Figure 2a**, the bridge CO band in the case of O+CO co-adsorption on coalesced NPs is similar in frequency (8 cm^{-1} redshift) and bandwidth to CO band without oxygen [**45**], indicating that the presence of O(ad) does not give rise to a large change of the coverage of CO on coalesced Pd(100) surface for an O_2/CO pressure ratio of 0.2, which agrees with the previous experiment shown in **Figure 1**. The small redshift of 8 cm^{-1} can be attributed to electrostatic interactions, leading to a deformation of CO electron cloud attracted by the neighbour O(ad) [**54**], which weakens C-O bond and therefore decreases the CO stretch frequency. In **Figure 2b** for 5.8 nm NPs, the bridge CO band is considerably redshifted by 32 cm^{-1} and broadened. In **Figure 2c,** a similar behavior with 5.8 nm NPs is observed for smaller NPs, but the frequency shift is reduced to 19 cm^{-1}. Based on the previous work, we know that for 5.8 nm large NPs, (100) facet extend is larger than for 3.6 nm large Pd NPs (Geometrical parameters of NPs are shown in **Figure S4** and **Table S1** in Supporting information). Thus, without O(ad) at equivalent CO coverage, a larger (100) facet, which contains more adsorbates, leads to a larger dipolar coupling, *i.e* a larger frequency shift, as demonstred in ref. [**10**]. Then the larger CO frequency redshift in the presence of O(ad) on 5.8 nm NPs can be plausibly attributed to the reduction of steady state CO coverage accounted to CO oxidation on Pd NPs by reducing more, relatively to smaller NPs, the dipolar coupling. In addition, compared with Pd(100) crystal or coalesced Pd(100) surface, the subsurface O can play an important role in Pd NPs. It was reported at 293 K that O can be incorporated into Pd NPs [**28**] but not into Pd single crystal surface [**50**]. O atom below Pd can modify the electronic states of the Pd atom in a way that enhances CO−Pd bonding strength [**55**], which agrees with the frequency redshift. The explanation of subsurface O in Pd NPs are also in agreement with SFG observation of the non-resonance (NR) signal (**Figure**

S1 in **Supporting Information**). The NR signal can be suppressed by the presence of oxygen in the case of NPs, however no effect is found on single crystal or coalesced NPs. Because the NR signal comes from the excitation of electronic states near Fermi level [**63**], the suppression of NR signal in the presence of O on NPs can be explained by the subsurface O which changes the electronic states near the Fermi level of Pd NPs. The broadening of CO bandwidth can be attributed to the superposition of CO bands on different (100) and (111) facets.

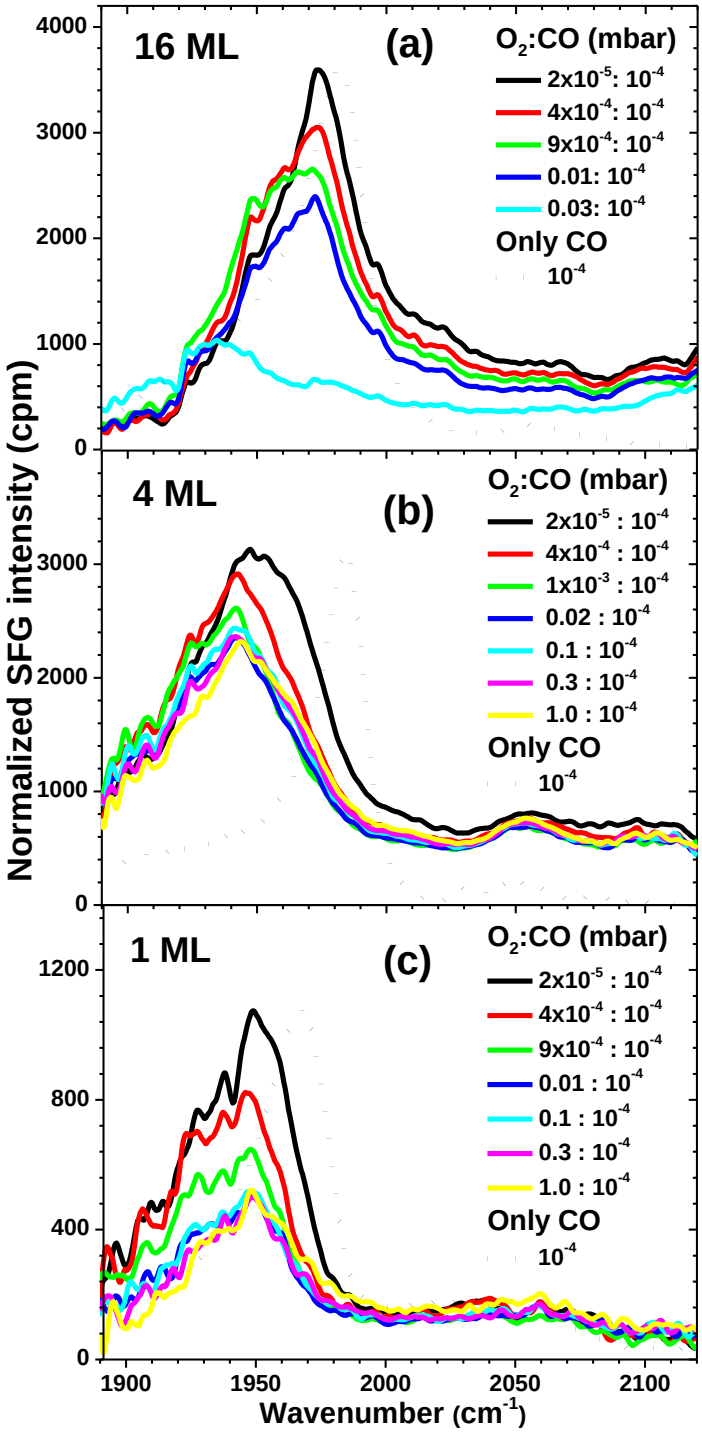

Figure 2. SFG spectra of CO (10^{-4} mbar) adsorbed on O_2 pre-treated NPs for three Pd equivalent thicknesses: (a) 16 ML; (b) 4 ML; (c) 1 ML as a function of O_2 pressure from 2×10^{-5} up to 1 mbar at 293 K. Dot curves show SFG CO spectra on Pd NPs without O_2.

In **Figure 2a**, during the increase of O_2 pressure from 10^{-5} to 10^{-2} mbar the CO band intensity at 1972 cm^{-1} is decreased by 40% and suddenly vanishes at 3×10^{-2} mbar. This is a clear evidence of CO oxidation on coalesced NPs for O_2/CO pressure ratio larger than 3×10^{2}, which is very close to the case of the single crystal (**Figure S2**). However a small coverage of bridge-bonded CO at 1929 cm^{-1} and linear CO at 2090 cm^{-1} remained. In **Figure 2b**, with an increase of O_2 pressure from 2×10^{-5} to 1×10^{-2} mbar, a 50% decrease of CO band is observed, along with a 10 cm^{-1} redshift. However, even an increase of O_2 up to 1 mbar could not remove completely CO from the surface. In **Figure 2c**, the intensity of bridged-bonded CO at 1952 cm^{-1} on 3.6 nm NPs is decreased of more than 70% upon an increase of O_2 pressure from 2×10^{-5} to 1×10^{-2} mbar and then remained constant until the O_2 pressure reached 1 mbar. This result is similar to that of 5.8 nm NPs. There are hence two types of bridge CO around 1950 cm^{-1}, one can be oxidized easily at $<10^{-3}$ mbar O_2 pressure, while the other one is more difficult to be oxidized. For both NP sizes, sample must be heated to oxidize the remaining CO.

As shown in **Figure 3a**, when the temperature reaches 316 K, the intensity of CO band at 1950 cm^{-1} is quickly reduced and the band at 1929 cm^{-1} remains constant up to 321 K. The disappearance of the band comes only from bridge CO on terrace (100), because the reactivity of other bridge sites on NPs is different. The stability of remaining CO is still not well understood, probably CO are adsorbed on defects or (111) facets of Pd NPs with a higher binding energy. The linear CO band seems not to change in this temperature and pressure range, although it has been reported to be the active sites for CO on Pd NPs on Al_2O_3 [**56**] or Pt NPs on SiO_2 and TiO_2 [**57**] at higher temperature (≥100 ºC). In **Figure 3b**, a similar behavior is found for 3.6 nm Pd, and the required temperature to oxidize CO is ~340 K. The decrease of SFG intensity induced by CO desorption during heating at the same temperature is up to 25% and 40% for large and small NPs respectively

(dash line in **Figure 4**). It confirms that CO disappearance for both NP sizes in **Figure 3** comes mainly from the CO oxidation. Unfortunately, in the relatively low temperature condition in our experiment (room temperature up to 340 K), CO_2 conversion is not efficient [**58**]. Limited by the sensibility of our mass spectroscopy and a design defect in the vacuum experimental setup, CO_2 production was not measured. However it is believed that the CO disappearance on Pd NPs comes mainly from CO oxidation, because the presence of O enhances the CO−Pd bonding [**55**], which has been proved by the CO band frequency redshift, therefore the O co-adsorption with CO would not induce the CO disappearance directly, so the only possibility comes from the CO oxidation.

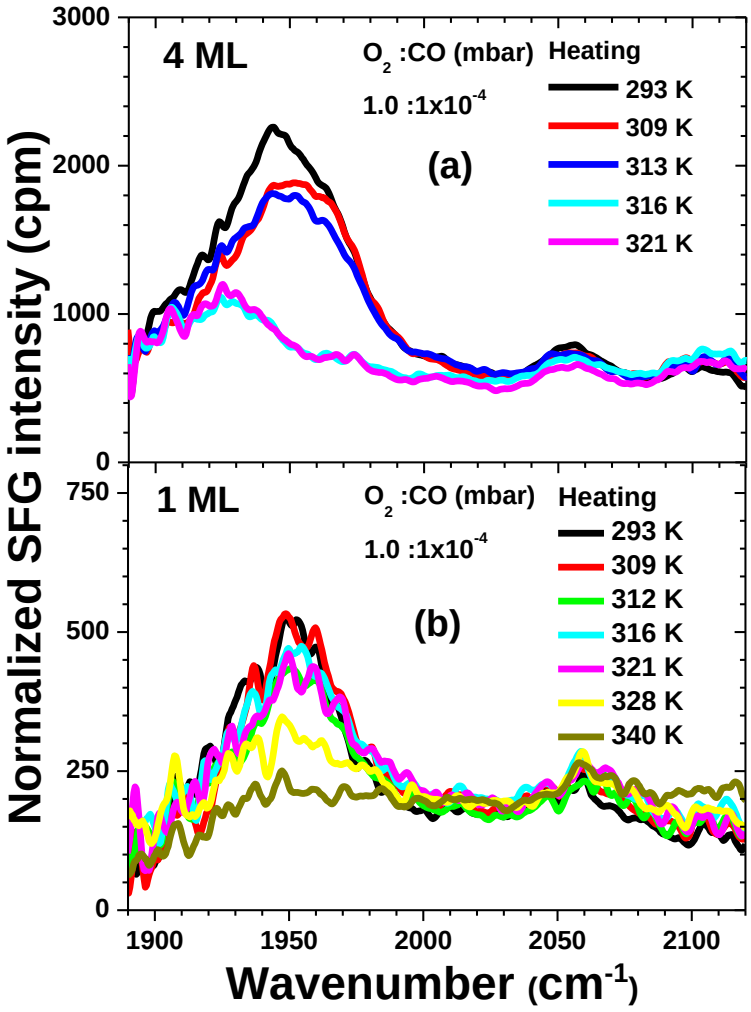

Figure 3. SFG spectra of CO (1×10^{-4} mbar) in the presence of 1.0 mbar of O_2 on (a) 5.8 nm NPs; (b) 3.6 nm NPs on MgO/Ag(100) upon heating.

We have combined SFG results of CO oxidation on Pd(100) and Pd NPs with different sizes at room temperature (**Figure 4a**) and upon heating (**Figure 4b**). It evidences the presence of two types of CO band at around 1950 cm^{-1} having different reactivity: the first one decreases at room temperature when the O_2 pressure raised from 10^{-5} to 10^{-2} mbar for NPs and Pd(100) (O_2/CO pressure ratio ~10^2) and is more obvious on smaller NPs. It was shown that oxygen preferentially accumulates at the edges of the NPs [**2**] or at the NP/substrate support interface [**25**]. NP edge sites with a lower coordination are believed to be more reactive than facet sites [**49**]. NP/substrate interface was also proposed as active sites for CO oxidation [**59, 60, 61**], however we could distinguish CO at interface from CO on NPs. Our results agree with the fact that smaller NPs with larger edge/facet ratio demonstrates higher reactivity. Therefore, CO oxidized at a low O_2 pressure at room temperature can be attributed to those on edge sites. The second one is attributed to CO on (100) facet of NPs, where a lower diffusion barrier leads to a sudden disappearance of amount of CO [**10, 47**] on large NPs or Pd(100), by continuously increasing the O_2 pressure. As shown in **Table S1**, the calculated $N_{terrace}/N_{edge}$ (N is atom number) is 2.3±0.5 and 1.3±0.3 for 5.8 and 3.6 nm NPs, respectively (Details of the calculation are shown in **Supporting Information**). The number of surface atoms corresponds to twice of available bridge adsorption sites for CO. By assuming an similar hyperpolarizability for CO on edges or facets, considering $I_{SFG} \propto N^2_{CO}$ [**37**], where I_{SFG} is the intensity of SFG signals and N_{CO} the surface number of CO, the results agree very well with intensity drops during CO oxidation for both the NP sizes up to 1 mbar O_2 at room temperature. It further confirms the assignment of reactive sites. During CO oxidation, more reactive edge sites should be transient and low-populated, as they are filled by CO diffusing from

facets and emptied again by oxidation. Actually in our previous work [**39**], the pump-probe experiment (10^{-4} mbar of CO adsorbed on 3.5 nm sized Pd deposited on 2 ML MgO/Ag(100) is pumped by 800 nm laser pulse and probed as function of time) has proved this kinetics process: in the absence of O_2, a decrease of the bridge CO and a growth of the CO at edges has been observed, however in the presence of O_2, the bridge CO band decreases with the excitation of pump but the CO band at edges has vanished [**39**].

By comparing the behavior of bridge CO band on Pd(100), coalesced, 5.8 and 3.6 nm Pd NPs we can state that the catalytic reactivity of CO on terrace (100) becomes less efficient with decreasing NP size. Higher O_2 pressure and temperature are necessary to remove CO for small NP sizes. This result can be explained by the increase of CO adsorption energy on terrace (100), corresponding to a decrease of frequency [**9**], in a good agreement with our previous results showing a decrease of CO singleton frequency for smaller NPs [**10**]. Indeed the epitaxial growth on MgO ultrathin film leads to strong geometrical deformations due to the large mismatch between Pd (3.96 Å) and MgO(100) (4.16 Å) lattices. The Pd layer at the interface in large NPs is expanded in the parallel plane by 3−4% relative to isolated NPs, while the upper layer is close to Pd bulk lattice due to strain releases within the NP. It gives rise to a CO adsorption energy closer to the case of Pd(100), while CO on terrace on a smaller NPs has a larger adsorption energy [**10**], because the terminal layer still experiences the lattice expansion induced by the support.

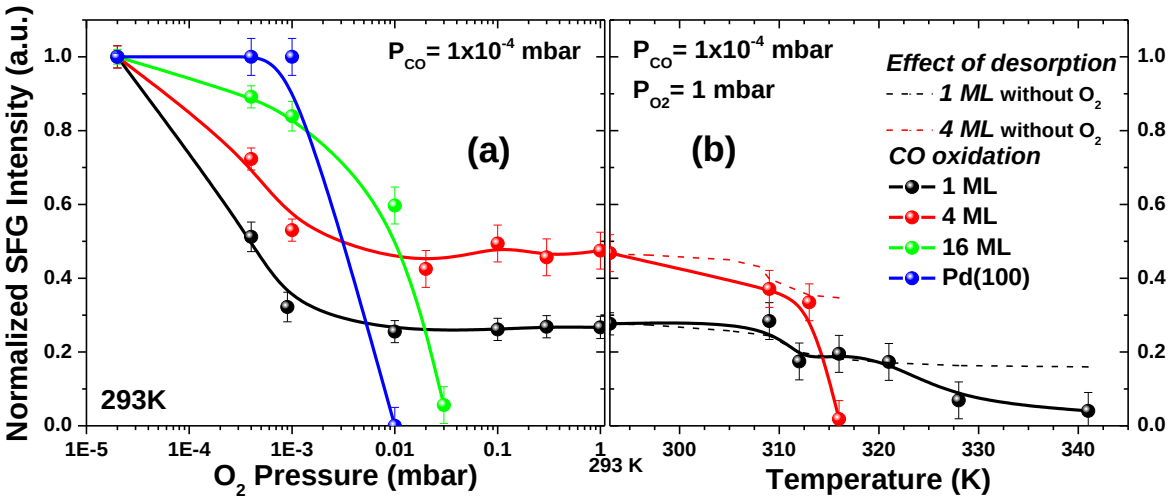

Figure 4. Normalized SFG intensities for catalytic oxidation of bridge CO band (points) on (100) facet of O_2 pre-treated Pd(100) single crystal (blue), coalesced (green), 5.8 nm (red) and 3.6 nm (black) Pd NPs, respectively. All the SFG intensities are obtained from spectral fitting, therefore the influence of non-resonant term and cross term between resonant peaks can be excluded. (a) At room temperature, $P_{CO}=1\times10^{-4}$ mbar and P_{O2} is varied from 2×10^{-5} to 1 mbar. (b) Effect of sample temperature (only for 5.8 and 3.6 nm NPs) under $P_{CO}=1\times10^{-4}$ mbar and $P_{O2}=1$ mbar. Lines are provided for guiding eyes. Dash lines correspond to CO band intensity induced by thermal desorption without O_2 on both Pd NP sizes.

On 3.6 nm Pd NPs the adsorption energy of CO on edges sites should have the similar behaviors, i.e. a larger adsorption energy for smaller NPs. However it is not observed experimentally because it is covered up by the quick increase of edge/facet ratio on smaller NPs. However, different from Pd NPs on MgO(100), the average Pd-Pd bond lengths for bare Pd cluster [**62**], Pd NPs deposited on Fe_3O_4 [**2**] and Al_2O_3 [**29**] support, has been reported decreasing with size, which can explain the decreased activation energy with Pd particle size in these cases [**31, 33**]. Therefore our results for CO reactivity trends are not in contradiction with the references [**15**, **31, 33**]. Consequently, the reactivity of CO on Pd NP/MgO(100) is site- and size-dependent. This mixture-property model gives rise to a non-monotonic reactivity trend of CO on Pd NPs. In the present work with different

NP sizes (3.6 nm, 5.8 nm, coalesced NPs) and Pd(100) single crystal, smaller Pd NPs exhibit a higher reactivity due to the increased edge/facet ratio, while larger NPs exhibit a higher reactivity due to larger terrace facet with smaller Pd-Pd atomic length at the NP surface and a lower diffusion barrier (**Figure 5**).

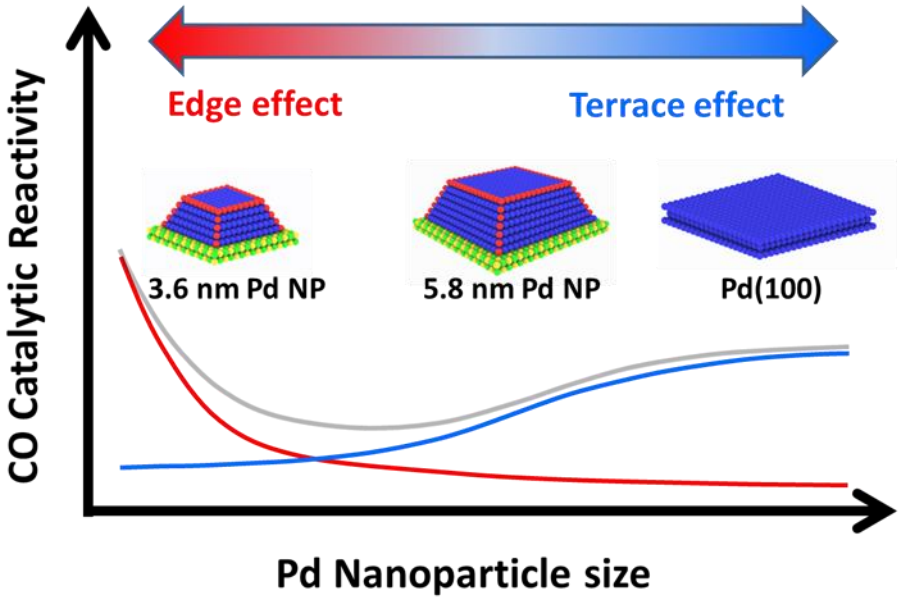

Figure 5. Schematic diagram of catalytic oxidation reactivity trends of bridge bonded CO on MgO(100) oxide supported Pd NP as a function of size. Red, blue and grey lines show a rough estimate of the contribution of edge, terrace sites and total, respectively.

Conclusion

This work applies vibrational SFG spectroscopy to study *in-situ* CO catalytic oxidation on MgO thin film supported Pd nanoparticles (NPs) compared to Pd(100) single crystal, under CO and O_2 pressures from UHV condition to the mbar range, temperatures from 293 to 340 K and NP average sizes from 3.6 nm up to their coalescence. On a Pd(100) single crystal at 293 K, CO oxidation process is found to prevail CO re-adsorption at the pressure ratio $O_2/CO \geq 3\times10^2$ on O_2 pre-exposed

Pd surface. At this pressure ratio, compressed CO phase (about 0.67 ML) limits reactivity (CO poisoning), but CO can be quickly removed by oxidation when CO coverage is lower than 0.5 ML. On Pd NPs, (1) the large changes of bridge CO bands in frequency and in width on 5.8 and 3.6 nm average diameter Pd NPs compared to CO adsorption bands without O_2 is caused by the presence of O(ad) and subsurface O into the NP at room temperature; (2) Under our experimental conditions, bridge sites (at edges and on facets) are the main active reaction sites compared to linear sites. (3) Observations suggest that the NP size and geometrical properties change the reactivity trend in different ways. The first one is the amount of low-coordination edge sites, which are more reactive than facet sites. The smaller the Pd NPs, the larger the edge/facet ratio and the higher the reactivity. The second one is the surface Pd-Pd bond length, which depends on NP size because of the large lattice difference between Pd and MgO. The larger the Pd NPs, the smaller the terrace Pd-Pd atomic length, and the higher the reactivity. The lower diffusion barrier on large facet also facilitate the reaction. The reactivity of CO on MgO(100)-supported Pd NPs is both site and size-dependent, this mixture component properties give rise to a non-monotonic reactivity trend of CO on Pd NPs. For perspective, further *in-situ* studies are needed to give a better understanding the CO catalytic oxidation behaviors on smaller Pd NPs and few atom clusters.

Conflicts of interest

There are no conflicts to declare.

Acknowledgment

We gratefully acknowledge the French National Agency for Research (Agence Nationale pour la Recherche, ANR) for financial support through the PNANO program (Project CANA ANR-06-

NANO-0031). We also acknowledge China Scholarship Council and National Natural Science Foundation of China (Grant No. 21701075) for the finance to Jijin Wang in France.

Reference

[1] G. Ertl, H. Knözinger, J. Weitkamp, , *Handbook of Heterogeneous Catalysis*; VCH: Weinheim, Germany, 1997.

[2] S. Schauermann, H.-J. Freund, *Acc. Chem. Res.* **2015**, 48, 2775-2782.

[3] T. Engel, and G. Ertl, et.al. *The chemical physics of solid surfaces and heterogeneous catalysis.* Elsevier. Amsterdam, Oxford, and New york, **1982**.

[4] M. J. Kale and P. Christopher, *ACS Catal.* 2016, 6, 5599−5609

[5] N. Alyabyeva, A. Ouvrard, A.-M. Zakaria, and B. Bourguignon, *J. Phys. Chem. Lett.* **2019**, 10, 624.

[6] N. Zheng, and G. D. Stucky, *J. Am. Chem. Soc.* **2006**, 128, 44, 14278-14280.

[7] M. Haruta, *Gold Bull.* **2004**, 37, 27.

[8] I. Stara, V. Nehasil, V. Matolin, *Surf. Sci.* **1996**, 365, 69.

[9] C. Goyhenex, M. Croci, C. Claeys, C. R. Henry, *Surf. Sci.* **1996**, 352, 475.

[10] A. Ouvrard, A. Ghalgaoui, C. Michel, C. Barth, J. J. Wang, S. Carrez, W. Q. Zheng, C. R. Henry, and B. Bourguignon, *J. Phys Chem. C*, **2017**, 121, 5551–5564.

[11] T. Schalow, B. Brandt, D. E. Starr, M. Laurin, S. K. Shaikhutdinov, S. Schauermann, J. Libuda, and H.-J. Freund, *Phys. Chem. Chem. Phys.*, **2007**, 9, 1347.

[12] Z. Li, S. F. Ji, Y. W. Liu, X. Cao, S. B. Tian, Y. J. Chen, Z. Q. Niu, and Y. D. Li, *Chem. Rev.* **2020**, 120, 623–682

[13] A. Wieckowski, E. R. Savinova, C. G. Vayenas, *Catalysis and Electrocatalysis at Nanoparticle Surfaces,* **2003**.

[14] D. Zemlyanov, B. Aszalos-Kiss, E. Kleimenov, D. Teschner, S. Zafeiratos, M. Haevecker, A. Knop-Gericke, R. Schlögl, H. Gabasch, W. Unterberger, K. Hayek, and B. Klötzer, *Surf. Sci.*, **2006**, 600, 983.

[15] Voogt, E. H., Mens, A. J. M., Gijzeman, O. L. J. and Geus, J. W., *Surf. Sci.*, **1997**, 373, 210–220.

[16] G. Ketteler, D. F. Ogletree, H. Bluhm, H. Liu, E. L. D. Hebenstreit, and M. Salmeron, *J. Am. Chem. Soc.*, **2005**, 127, 18269.

[17] J. Lin, X. D. Wang, T. Zhang, *Chin. J. Catal.* 37 (2016) 1805–1813

[18] H. Gabasch, A. Knop-Gericke, R. Schlögl, M. Borasio, C. Weilach, G. Rupprechter, S. Penner, B. Jenewein, K. Hayek, B. Klötzer, *Phys. Chem. Chem. Phys.*, **2007**, 9, 533-540.

[19] H. Conrad, G. Ertl, and J. Küppers, *Surf. Sci.*, **1978**, 76, 323.

[20] B. C. Gates, *Catalytic Chemistry*; John Wiley & Sons, Inc., New York, Singapore, **1992**.

[21] P. D. Nolan, B. R. Lutz, P. L. Tanaka, C. B. Mullins, *Surf.Sci.* **1998**, 419, L107−L113.

[22] S. M. Lang, I. Fleischer, T. M. Bernhardt, R. N. Barnett, and U. Landman, *ACS Catal.* **2015**, 5, 2275−2289.

[23] S. Penner, P. Bera, S. Pedersen, L. T. Ngo, J. J. W. Harris, C. T. Campbell, *J. Phys. Chem. B* **2006**, 110, 24577−24584.

[24] S. Shaikhutdinov, M. Heemeier, J. Hoffmann, I. Meusel, B. Richter, M. Bäumer, H. Kuhlenbeck, J. Libuda, H.-J. Freund, R. Oldman, S. D. Jackson, C. Konvicka, M. Schmid, P. Varga, *Surf. Sci.* **2002**, 501, 270−281.

[25] T. Schalow, M. Laurin, B. Brandt, S. Schauermann, B. Guimond, H. Kuhlenbeck, D. E. Starr, S. K. Shaikhutdinov, J. Libuda, H.-J. Freund, *Angew. Chem., Int. Ed.* **2005**, 44, 7601−7605.

[26] L. C. Liu, D. M. Meira, R. Arenal, P. Concepcion, A. V. Puga, and A. Corma, *ACS Catal.* **2019**, 9, 10626−10639

[27] G. Sitja, and C. R. Henry, *J. Phys. Chem. C* **2021**, 125, 24, 13247-13253

[28] I. Meusel, J. Hoffmann, J. Hartmann, M. Heemeier, M. Bäumer, J. Libuda, H.-J. Freund, *Catal. Lett.*, **2001**, 71, 5.

[29] S. A. Nepijko, M. Klimenkov, M. Adelt, H. Kuhlenbeck, R. Schlögl, and H.-J. Freund, *Langmuir***, 1999**, *15*, 5309.

[30] T. Engel, G. Ertl, *J. Chem. Phys.* **1978**, 69, 1267-1281.

[31] I. Stará, V. Nehasil, V. Matolín, *Surf. Sci.* **1995**, 331−333, 173−177.

[32] C. R. Henry, C. Chapon, C. Goyhenex, *Surf. Sci.* **1992**, 272, 283.

[33] I. Stará, V. Matolín, *Surf. Sci.* **1994**, 313, 99−106.

[34] J.-H. Fischer-Wolfarth, J. A. Farmer, J. M. Flores-Camacho, A. Genest, I. V. Yudanov, N. Rösch, C. T. Campbell, S. Schauermann, H.-J. Freund, *Phys. Rev. B*, **2010**, 81, 241416.

[35] N. Podda, M., Corva, F. Mohamed, Z. Feng, C. Dri, F. Dvorák, V. Matolin, G. Comelli, M. Peressi, and E. Vesselli, *ACS Nano* **2017**, 11, 1041.

[36] P. Guyot-Sionnest, , J. H. Hunt, and Y. R. Shen, *Phys. Rev. Lett.* **1987**, 59, 1597.

[37] H.-F. Wang, W. Gan , R. Lu , Y. Rao, B.-H. Wu, *International Reviews in Physical Chemistry*, 24, 191-256, (2005).

[38] A. Ghalgaoui, A. Ouvrard, J. J. Wang, S. Carrez, W. Zheng, and B. Bourguignon, *J. Phys. Chem. Lett.* **2017**, 8, 2666.

[39] A. Ghalgaoui, R. Horchani, J. J. Wang, A. Ouvrard, S. Carrez, and B. Bourguignon, *J. Phys. Chem. Lett.* **2018**, 9, 5202.

[40] G. Rupprechter, *Adv. Catal.* **2007**, 51,133.

[41] G. A. Somorjai, and G. Rupprechter, *J. Phys. Chem. B,* **1999**, 103, 1623.

[42] F. Liu, H.-L. Han, L. M. Carl, D. Zherebetskyy, K. An, L.-W. Wang, G. A. Somorjai, *J. Phys. Chem. C*, **2019**, 123,13, 7577-7583.

[43] H. Wang, A. Sapi, C. M. Thompson, F. Liu, D. Zherebetskyy, J. M. Krier, L. M. Carl, X. Cai, L.-W. Wang, G. A. Somorjai, *J. Am. Chem. Soc.*, **2014**, 136, 29, 10515-10520.

[44] A. Ouvrard, J. Niebauer, A. Ghalgaoui, C. Barth, C. R. Henry, and B. Bourguignon, *J. Phys Chem. C*, **2011**, 115, 8034.

[45] A. Ouvrard, J. J. Wang, A. Ghalgaoui, S. Nave, S. Carrez, W. Q. Zheng, H. Dubost, and B. Bourguignon, *J. Phys. Chem. C*, **2014**, 118, 19688.

[46] Q.-L. Guo, and P. J. Møller, *J. Phys. Chem. C*, **2010**, 114, 18167.

[47] O. H. Pakarinen1, C. Barth, A. S. Foster, and C. R. Henry, *J. Appl. Phys.* **2008**, 103, 054313.

[48] R. Toyoshima, M. Yoshida, Y. Monya, K. Suzuki, B. S. Mun, K. Amemiya, K. Mase, and H. Kondoh, *J. Phys. Chem. Lett*. 2012, 3, 3182−3187

[49] H. Falsig, B. Hvolbæk, I. S. Kristensen, T. Jiang, T. Bligaard, C. H. Christensen, and J. K. Nørskov, *Angew. Chem. Int. Ed*, **2008** ,47, 4835–4839.

[50] F.P. Leisenberger, G. Koller, M. Sock, S. Surnev, M. G. Ramsey, F. P. Netzer, B. Klötzer, K. Hayek, *Surf. Sci.,* **2000**, 445, 380.

[51] A. P. Seitsonen, Y. D. Kim, S. Schwegmann, and H. Over, *Surf. Sci.* **2000**, 468, 176.

[52] H. Over, *Prog. Surf. Sci.* **1998**, 58, 249.

[53] S. Bertarione, D. Scarano, A. Zecchina, V. Johanek, J. Hoffmann, S. Schauermann, M. M. Frank, J. Libuda, G. Rupprechter, and H.-J. Freund, *J. Phys Chem. B,* 2004, 108, 3603.

[54] W. Liu, Y. F. Zhu, J. S. Lian, and Q. Jiang, *J. Phys. Chem. C*, 2007, 111, 1005-1009

[55] V. Mehar, M. Kim, M. Shipilin, M. V. Bossche, J. Gustafson, L. R. Merte, U. Hejral, H. Grönbeck, E. Lundgren, A. Asthagiri, and J. F. Weaver, *ACS Catal.* 2018, 8, 8553−8567

[56] K. Murata, E. Eleeda, J. Ohyama, Y. Yamamoto, S. Arai and A. Satsuma， *Phys. Chem. Chem. Phys.*, **2019**, 21, 18128

[57] K. Ding, A. Gulec, A. M. Johnson, N. M. Schweitzer, G. D. Stucky, L. D. Marks and P. C. Stair, *Science*, **2015**. 350, 189–192.

[58] P. J. Berlowitz, C. H. F. Peden, and D. W. Goodman, *J. Phys. Chem.* **1988**, 92, 5213-5221

[59] Q. Fu, F. Yang, and X. Bao, *Acc. Chem. Res.*, **2013**, 46, 1692.

[60] B. Yoon, and U. Landman, *J. Phys. Chem. C*, **2012**, 116, 9594-9607.

[61] Y. Suchorski, S. M. Kozlov, I. Bespalov, M. Datler, D. Vogel, Z. Budinska, K. M. Neyman, and G. Rupprechter, *Nature Materials*, **2018**, 17, 519–522

[62] S. Krüger, S. Vent, F. Nörtemann, M. Staufer, and N. Rösch, *J. Chem. Phys.* **2001**,115, 2082.

[63]A. D. Curtis, S. R. Burt, A. R. Calchera, and J. E. Patterson, J. Phys. Chem. C 115, (2011) 11550–11559

[64] J. J. Wang, H. Dubost, A. Ghalgaoui, W. Zheng, S. Carrez, A. Ouvrard, B. Bourguignon, Surf. Sci. 626 (2014) 26–39